

Disentangling oxidation/hydrolysis reactions of brain mitochondrial cardiolipins in pathogenesis of traumatic injury

Honglu Chao,^{1,2,3} Tamil S. Anthonymuthu,^{1,2} Elizabeth M. Kenny,^{1,2} Andrew A. Amoscato,⁴ Laura K. Cole,⁵ Grant M. Hatch,⁵ Jing Ji,^{1,2,3} Valerian E. Kagan,^{4,6} and Hülya Bayır^{1,2,5}

¹The Safar Center for Resuscitation Research and the Neuroscience Institute of Children's Hospital of Pittsburgh of University of Pittsburgh Medical Center, Pittsburgh, Pennsylvania, USA. ²Department of Critical Care Medicine, University of Pittsburgh School of Medicine, Pittsburgh, Pennsylvania, USA. ³Department of Neurosurgery, The First Affiliated Hospital of Nanjing Medical University, Nanjing, China. ⁴Center for Free Radical and Antioxidant Health, Department of Environmental and Occupational Health, University of Pittsburgh, Pittsburgh, Pennsylvania, USA. ⁵Diabetes Research Envisioned and Accomplished in Manitoba, Children's Hospital Research Institute of Manitoba, Department of Pharmacology and Therapeutics, Faculty of Health Sciences, University of Manitoba, Winnipeg, Canada. ⁶Laboratory of Navigational Redox Lipidomics, Institute of Regenerative Medicine, IM Sechenov Moscow State Medical University, Moscow, Russia.

Mechanical injury to the brain triggers multiple biochemical events whose specific contributions to the pathogenesis define clinical manifestations and the overall outcome. Among many factors, mitochondrial injury has recently attracted much attention due to the importance of the organelle for bioenergetics as well as intra- and extracellular signaling and cell death. Assuming the essentiality of a mitochondria-unique phospholipid, cardiolipin (CL), for the structural and functional organization of mitochondria, here we applied global (phospho) lipidomics and redox lipidomics to reveal and identify CL modifications during controlled cortical impact (CCI). We revealed 2 major pathways activated in the CCI-injured brain as time-specific responses: early accumulation of oxidized CL (CLOx) products was followed by hydrolytic reactions yielding monolyso-CLs (mCLs) and free fatty acids. To quantitatively assess possible specific roles of peroxidation and hydrolysis of mitochondrial CL, we performed comparative studies of CL modifications using an animal model of Barth syndrome where deficiency of CL reacylation (Tafazzin [Taz] deficiency) was associated exclusively with the accumulation of mCLs (but not CLOx). By comparing the in vitro and in vivo results with genetic manipulation of major CL-, CLOx-, and mCL-metabolizing enzymes, calcium-independent phospholipase A₂γ and Taz, we concluded that the 2 processes – CL oxidation and CL hydrolysis – act as mutually synergistically enhancing components of the pathogenic mechanism of mitochondrial injury in traumatic brain injury. This emphasizes the need for combined therapeutic approaches preventing the formation of both CLOx and mCL.

Authorship note: HC and TSA contributed equally to this work.

Conflict of interest: The authors have declared that no conflict of interest exists.

License: Copyright 2018, American Society for Clinical Investigation.

Submitted: September 25, 2017

Accepted: September 19, 2018

Published: November 2, 2018

Reference information:

JCI Insight. 2018;3(21):e97677.

<https://doi.org/10.1172/jci.insight.97677>.

insight.97677.

Introduction

The enormous complexity of brain functions requires a highly effective coordination of multiple metabolic reactions via extremely sophisticated signaling. Ruthless demolition of this harmonized organization — in the limited volume of the brain — creates chaos: discoordination of many usual regulatory processes and triggering of abnormal reactions that engage newer anatomical areas and enhance the overall damage over time. The incidence of brain trauma in pediatric, adult, and geriatric populations shows continuous growth (1, 2). Thus, the urgently required therapeutic strategies necessitate identification of the leading pathogenic pathways as the targets for new drug discovery.

Mitochondria — with their established critical role in bioenergetics and newly appreciated role in signaling — have emerged as one of the leading hubs where many of the disastrous reactions of trauma pathogen-

esis are initiated (3, 4). Essential for both structural organization and regulatory functions of mitochondria is their unique phospholipid, cardiolipin (CL), normally confined almost exclusively to the matrix leaflet of the inner mitochondrial membrane (IMM; refs. 5–8). Collapse of CL asymmetry along with aberrant metabolism — oxidative modification and hydrolysis — are believed to be inherently involved in the chain of pathogenic events leading to erroneous signaling, weakening the healing process and worsening the overall prognosis (7, 9, 10). Two major types of reactions — oxygenation of CLs (catalyzed predominantly by an intramembrane space hemoprotein, cytochrome c; ref. 11) and enzymatic hydrolysis of nonoxidized CLs by various phospholipase(s) A_2 and of CLOx predominantly by calcium-independent phospholipase $A_2\gamma$ (iPLA $_2\gamma$; refs. 12, 13) — may be closely intertwined with each other, yielding a synergistically enhanced, injurious reaction network that is propagated in the aftermath of the traumatic event. The large number of individual molecular products generated by both processes makes the task of their identification daunting, thus discouraging experimental work and drug design and development in this area (14). Our previous work using high-resolution liquid chromatography–mass spectrometry (LC-MS) has definitively characterized more than 150 individual oxidized CL (CLOx) products generated in traumatized brain tissue (14). A more recent study (15) added another approximately 700 individual oxygenated polyunsaturated fatty acids as potential participants in trauma-initiated damage. Intriguingly, a mitochondria-targeted scavenger of electrons, XJB-5-131, was protective against traumatic injury not only in the context of biochemical characteristics, but also in functional outcomes (16). This emphasizes the role and contribution of the redox component of lipid oxidation in the overall damage.

The role of hydrolytic reactions as enhancers or quenchers of the damage and their potentially nonlinear interactions with the redox reactions remains unknown. As a potentially useful approach to quantitative assessments of these complex interactions, we chose to use a model of a monogene brain impairment — Tafazzin (Taz) deficiency — which is associated with only 1 of the above processes — aberrant hydrolytic metabolism of CL and accumulation of CL hydrolysis products, monolyso-CLs (mCLs), due to ineffective reacylation of the hydrolytic products by the essential acyltransferase Taz (17–20). Here we quantitatively assessed, for the first time to our knowledge, the possible specific roles of peroxidation and hydrolysis of mitochondrial CLs and present evidence that these 2 processes act as mutually enhancing components of the pathogenic mechanism of mitochondrial injury in traumatic brain injury (TBI).

Results

TBI causes accumulation of CLOx and mCLs. To obtain detailed knowledge about the TBI-induced changes in CL metabolism, we performed a high-resolution redox phospholipidomics time course analysis of CLs and their major redox and hydrolytic metabolites. The total CL content in the cortical contusion zone decreased at 1, 4, and 24 hours after TBI versus control, whereby the effect was particularly robust at 4 hours (Figure 1A). To quantitatively assess the alterations in the levels of molecular species of CL, we constructed contour maps of changes in CL content after TBI relative to their levels in the control group (Figure 1B). We found that both polyunsaturated and saturated CL species were decreased at 1 hour, whereas predominantly polyunsaturated CL species were decreased at 4 hours. Finally, at 24 hours, the low-molecular-weight CL species containing polyunsaturated fatty acids (PUFAs) were reduced whereas CL species with longer acyl chains (and respectively higher masses) were substantially increased. Comparing the changes with the total unsaturation pointed toward a quadratic correlation indicating that PUFA-containing CLs were removed at a much higher rate than their saturated counterparts. This trend was observed at all 3 time points, however, with varying intensity: a strong correlation at 4 hours, a moderate correlation at 24 hours, and a modest correlation at 1 hour (Figure 2A). Overall, these data revealed highly specific patterns of PUFA-containing CL responses and changes in molecular speciation of CLs in the injured brain.

We further determined the amount of oxidatively modified CLs at different time points after TBI. The total amount of CLOx peaked (>3.5-fold) at 1 hour after TBI, and elevated CLOx levels were detected at later time points (4 and 24 hours) versus the control group (Figure 1A). Regarding molecular speciation of CLOx, the following specific features were established: (a) most of the CL species were oxidized to a similar extent at 1 hour; (b) the CLOx species with PUFAs were sequentially decreased at 4 and 24 hours while the CLOx species containing saturated or monounsaturated fatty acyls largely remained unchanged (Figure 2B).

TBI also caused elevation of mCL content; however, the time course was markedly different from CL oxidation — a slight increase at the earlier time point (1 hour) and a greater increase (>2.5-fold) at both 4 and 24 hours (Figure 1A). At 1 hour, the changes were prevalent across all saturated and unsaturated

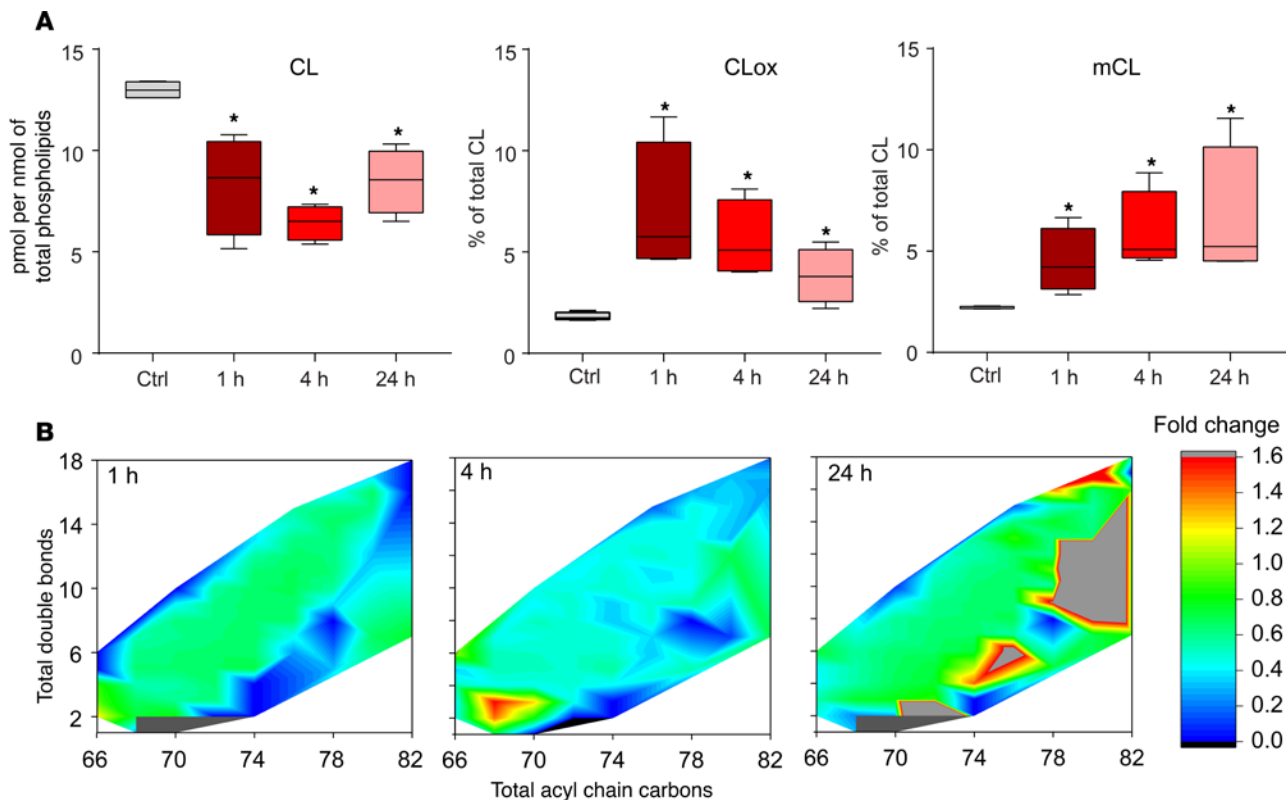


Figure 1. Time course analysis of CL profile in the brain after TBI by LC-MS. (A) Quantitative assessment by LC-MS of total CL, CLox, and mCL content in the contusional cortex at 1, 4, and 24 hours after controlled cortical impact (CCI). $n = 4/\text{group}$, $*P < 0.05$ vs. control, 1-way ANOVA. The box plots depict the minimum and maximum values (whiskers), the upper and lower quartiles, and the median. The length of the box represents the interquartile range. **(B)** Color contour map showing changes in CL species at 1, 4, and 24 hours with respect to control. Values are average from 4 animals.

species whereas there was a noticeable, steady increase in species containing less than 7 total double bonds at 4 and 24 hours (Figure 2B). These results are compatible with the formation of mCLs via hydrolysis of PUFAs or oxygenated PUFAs at 4 and 24 hours after the injury.

Overall, the specific features of the temporal changes suggest that redox reactions leading to the accumulation of CLox preceded the hydrolysis of CL and/or CLox. To get better insight into the interrelationships between the 2 types of TBI-dependent CL modifications, namely oxidation and hydrolysis, we constructed chord diagrams revealing correlations between the changes of the CL oxidation and hydrolysis products (Figure 2B). We found that the interconnectivity of the formation of CLox and mCL was already observed at 1 hour after TBI and progressively increased at 4 and 24 hours after the injury. Notably, multiple CLox species correlated with the formation of mCL species at 1 hour. However, at later time points, CLox species formed from the PUFA-containing CLs (with greater than 8 double bonds) strongly correlated with mCL formation. These results point to a random CL hydrolysis at 1 hour and a more specific and selective hydrolysis of oxidized PUFA at later time points.

The paramount differences between the CLox and mCL responses are likely reflective of the steady-state levels of these intermediates contributing to the initial, severe mechanical damage and substantial apoptosis in cortical neurons and subsequent attempts to repair via the activation of the 2 major proteins of CL remodeling — iPLA₂γ (known to remove the oxygenated PUFA from CLox) as well as Taz that reacylates the iPLA₂γ-generated mCLs. The results reveal that the first part of the repair machinery was very effective (Supplemental Figure 1A; supplemental material available online with this article; <https://doi.org/10.1172/jci.insight.97677DS1>) — the initial huge spike in the amount of CLox was leveled off to a much lower amount. This corresponds very well with an increase in iPLA₂γ expression at 1 and 4 hours and its leveling off back to the control values at the latest tested time (24 hours) (Figure 3A).

On the other hand, a significant increase in the expression levels of Taz — the catalyst of the major phospholipid reacylation process in CLs (21, 22) — was observed at 4 and 24 hours compared with 1 hour (Figure

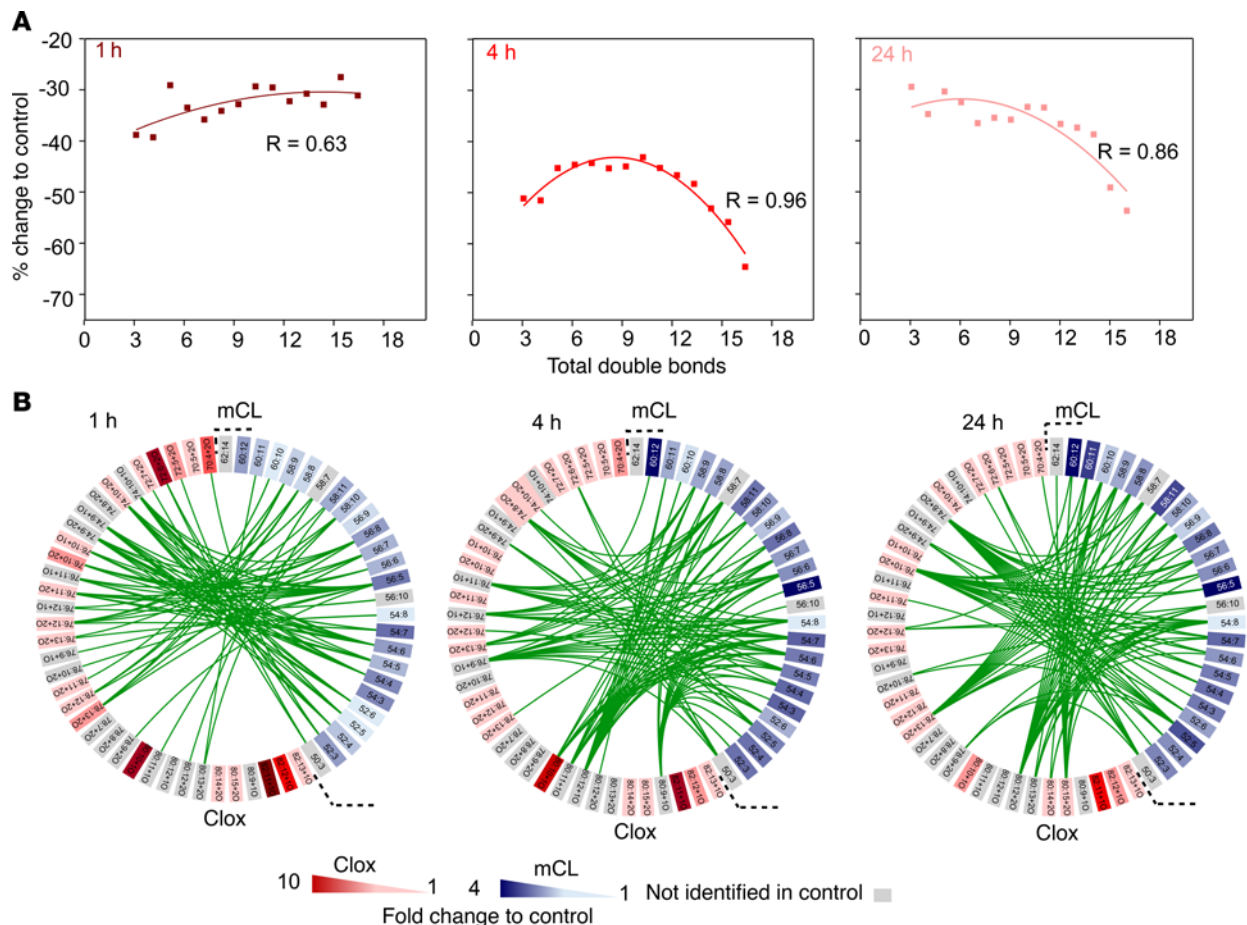


Figure 2. Correlation analysis of changes in CL after TBI. (A) Correlation of changes in CL content between control and 1-, 4-, or 24-hour samples and the total number of double bonds. **(B)** Chord diagram showing the correlation between CLox and mCLs. The connecting chord represents a Spearman's correlation coefficient greater than 0.6 between CLox and mCLs. Values are average from 4 animals.

3B). This characteristic behavior was also observed after mechanical stretch injury in neurons (Supplemental Figure 1B) whereby transient increase of $iPLA_2\gamma$ and a delayed increase of Taz expression at 36 hours after the injury were detected as well (Figure 3, C and D). Finally, the same pattern of strong and consistent activation of Taz expression was also characteristic for several cases of human TBI whereby both at 6 and 48 to 72 hours, the levels of Taz protein were significantly increased (Figure 3E and Supplemental Figure 1C) after the insult.

mCL accumulation in the brain of Taz-deficient mice. Assuming that reacylation represents the “bottleneck” of the overall remodeling process, we further chose to study the Taz-driven hydrolysis/remodeling of brain CLs in Taz-deficient animals. Such an approach gives the advantage of better understanding the hydrolysis/reacylation reactions uncomplicated by the simultaneous redox modifications of CL and the formation of CLox species. Indeed, we found that in Taz-knockdown (Taz-KD) mice, a robust accumulation of mCLs occurred, resulting in a slight but significant ($P < 0.05$ vs. WT) depletion of CL (Figure 4, A and B). In terms of molecular speciation of accumulated mCL species and lost CL species (Figure 4, C and D), the major loss was found in CL species with multiple PUFAs. The CL species with 6 to 11 double bonds and 74 to 78 total acyl carbons showed a moderate decrease while the CL species with saturated fatty acids showed an increase (Figure 4C). Similarly, a greater increase among mCL species was found in PUFA-containing species (Figure 4D). The free fatty acid (FFA) analysis revealed a significant increase in arachidonic acid levels in the KD mice while the amounts of saturated FFAs, such as palmitic acid and stearic acid, were significantly lower (Figure 4E). Taz catalyzes the reacylation reaction after hydrolysis by one of the phospholipases A_2 . The latter reaction defines the levels of fatty acids released. As expected, the amounts of oxidized FFA species were also lower in the KD mice (Supplemental Figure 2). Taken together, the majority of the CL losses observed in Taz-deficient animals were due to the loss of PUFAs, such as

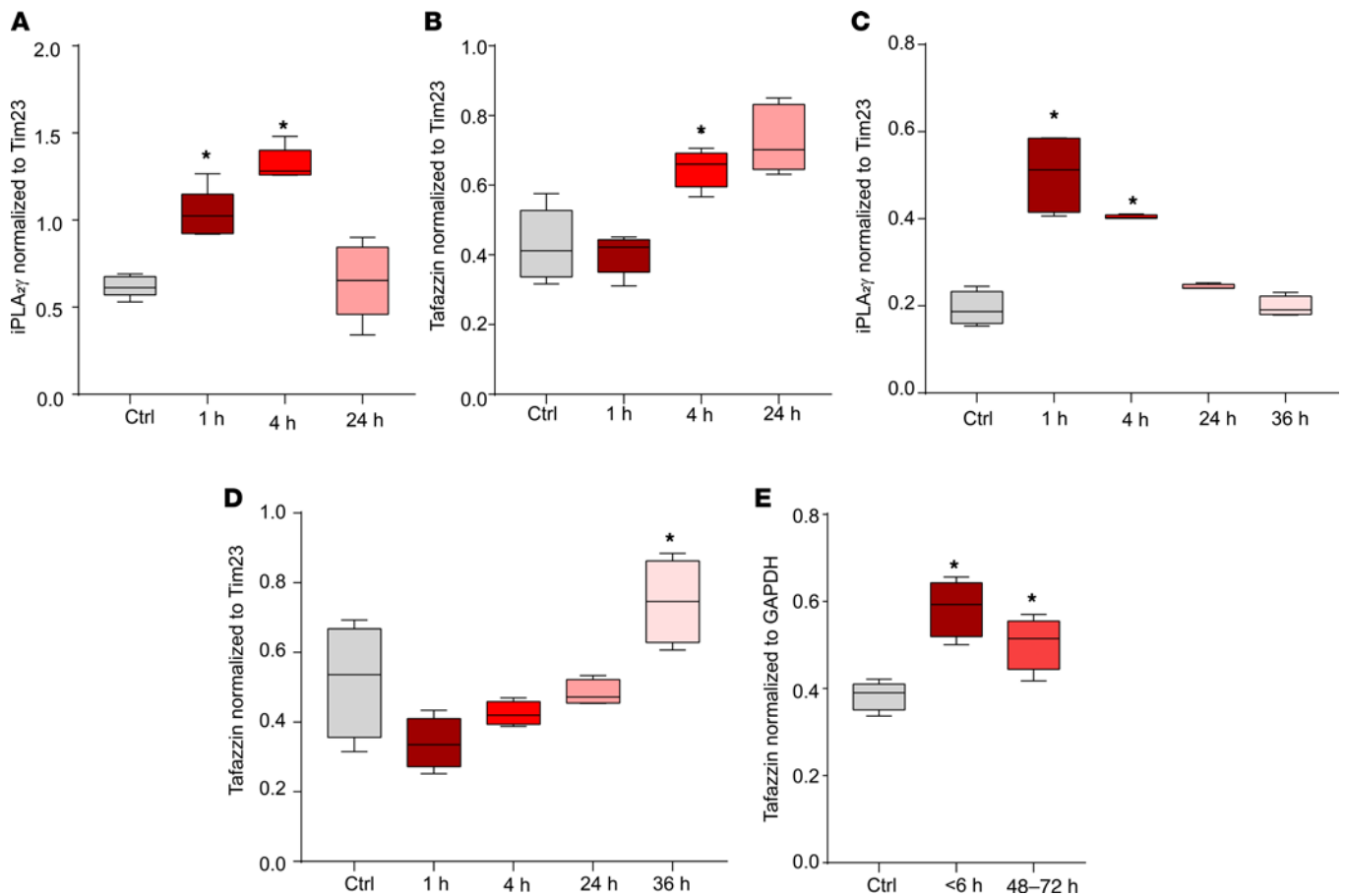


Figure 3. Evaluation of CL remodeling pathway proteins following TBI. (A) Expression levels (relative to mitochondrial marker Tim23) of the CL-remodeling protein iPLA₂γ after CCI in the contusional cortex. $n = 5/\text{group}$, $*P < 0.05$ vs. control, 1-way ANOVA. The box plots depict the minimum and maximum values (whiskers), the upper and lower quartiles, and the median. The length of the box represents the interquartile range. (B) Expression levels (relative to mitochondrial marker Tim23) of the CL-remodeling protein Taz after CCI in the contusional cortex. $n = 5/\text{group}$, $*P < 0.05$ vs. control, 1-way ANOVA. (C) Temporal profile of changes in the CL-remodeling protein iPLA₂γ (relative to mitochondrial marker Tim23) after mechanical stretch in HT22 cells. $n = 4/\text{group}$, $*P < 0.05$ vs. control, 1-way ANOVA. (D) Temporal profile of changes in the CL-remodeling protein Taz (relative to mitochondrial marker Tim23) after mechanical stretch in HT22 cells. $n = 4/\text{group}$, $*P < 0.05$ vs. control, 1-way ANOVA. (E) Changes in Taz expression (relative to GAPDH) in human contusional brain tissue for TBI patients who underwent resection of contusion within 6 hours or 48 to 72 hours after TBI. $n = 5/\text{group}$, $*P < 0.05$ vs. control, 1-way ANOVA.

arachidonic, docosapentaenoic, and docosahexaenoic acids. Notably, the correlation between the losses in CL species and the double bonds showed a second-order polynomial correlation (Figure 4F).

Levels of Taz expression define sensitivity of neurons to stretch injury. To more quantitatively assess the importance of Taz-dependent reacylation in neuronal cell injury and repair, we used mechanical stretch injury in HT22 cells transfected with iPLA₂γ known to hydrolyze both oxygenated and non-oxygenated phospholipids in mitochondria (15, 23, 24). This transfection markedly increased sensitivity of neuronal cells to stretch-induced injury (Figure 5, A and B, and Supplemental Figure 3A). We then performed the experiments with stretch injury in cells with manipulated levels of Taz expression (Supplemental Figure 3B). Remarkably, decreased levels of Taz were associated with increased sensitivity of cells to stretch-induced injury (Figure 5C) whereas elevated levels of Taz were associated with increased resistance to stretch-induced injury (Figure 5D). Assessments of mitochondrial integrity using a potential-sensitive fluorescent probe, JC-1, revealed that Taz levels were essential for preserving the polarized state of mitochondria impaired by stretch injury (Figure 5E).

Taz deficiency enhances rotenone-induced injury of neurons. We further employed another model of neuronal cell injury using a mitochondrial respiratory complex I inhibitor, rotenone (25, 26). Rotenone's ability to injure neuronal cells has been associated with the enhanced production of reactive oxygen species and oxidation/hydrolysis of CL and CLox (27–30). In this model, elevated levels of Taz induced protection (Figure 6A). Accordingly, Taz deficiency induced increased sensitivity to cell cytotoxicity (Figure 6B) and the loss of mitochondrial membrane potential (Figure 6C).

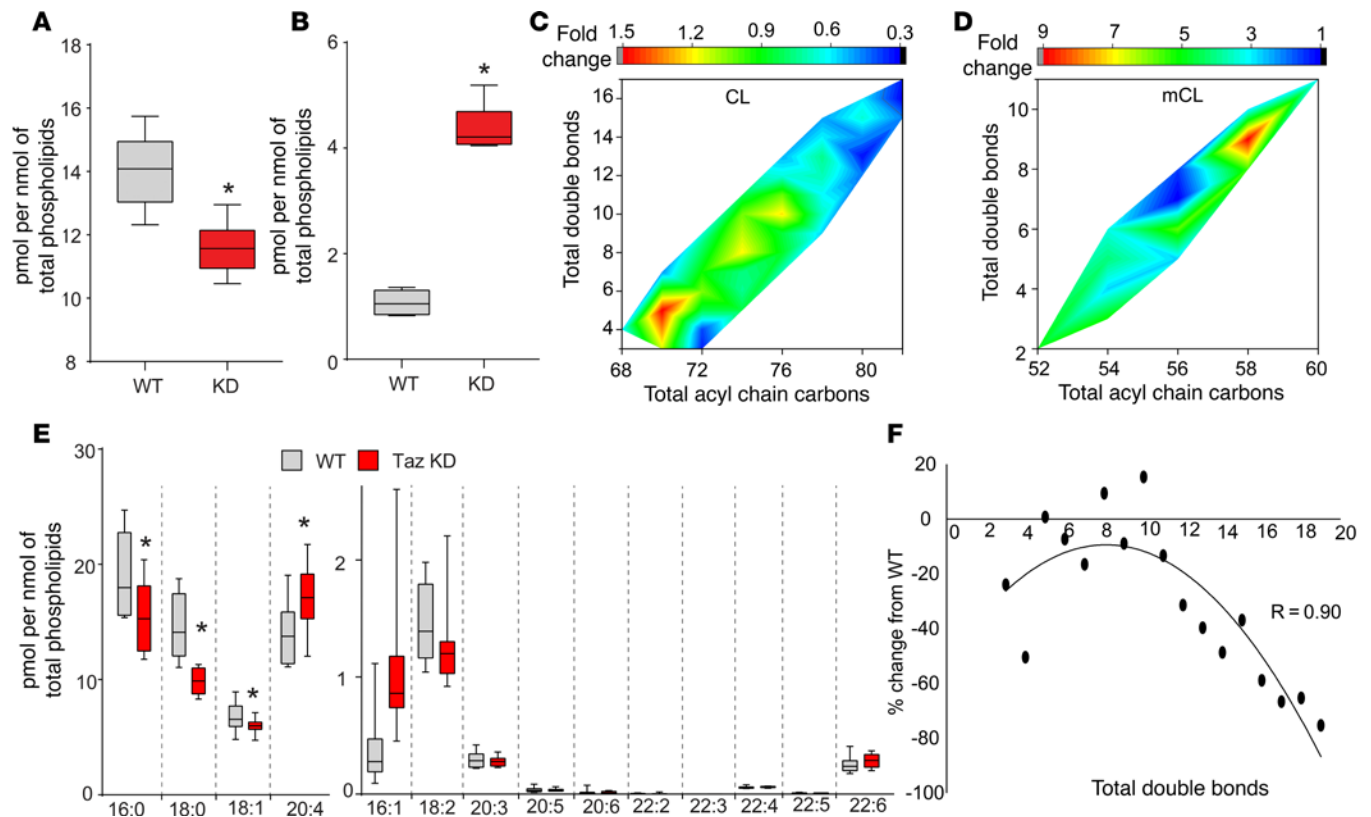


Figure 4. Changes in brain CL in Taz-KD mice. (A) Quantitative assessment of total amount of CLs in the brains of WT and Taz-KD mice. $n = 8/\text{group}$ and $*P < 0.05$ vs. WT, 2-tailed Student's t test. The box plots depict the minimum and maximum values (whiskers), the upper and lower quartiles, and the median. The length of the box represents the interquartile range. (B) Total amount of mCLs in the brains of WT and Taz-KD mice. $n = 8/\text{group}$ and $*P < 0.05$ vs. WT, 2-tailed Student's t test. The box plots depict the minimum and maximum values (whiskers), the upper and lower quartiles, and the median. The length of the box represents the interquartile range. (C) Color contour map showing changes in CL in Taz-KD mouse brain compared with WT mouse brain. (D) Color contour map showing changes in mCL in Taz-KD mouse brain compared with WT mouse brain. Values are average from 8 animals. (E) Assessment of free fatty acid content in WT and Taz-KD mouse brain. $n = 8/\text{group}$ and $*P < 0.05$ vs. WT, 2-tailed Student's t test. The box plots depict the minimum and maximum values (whiskers), the upper and lower quartiles, and the median. The length of the box represents the interquartile range. (F) Correlation between changes in CL levels in Taz-KD mice (compared with WT) and the total number of double bonds. There was a strong correlation between these 2 parameters ($R = 0.9$). Values are average from 8 animals.

Deficiency of iPLA₂γ attenuates TBI-induced neuronal death and behavioral deficits. Because iPLA₂γ plays a major role in hydrolyzing oxidatively modified CLs, we next evaluated the effect of iPLA₂γ knock down using the siRNA approach in vivo on neuronal death and behavioral deficits induced by CCI in rats. iPLA₂γ expression was significantly reduced in the KD animals versus the SC group (Figure 7A and Supplemental Figure 4). To assess neuronal injury, we employed FJC staining, commonly used to detect degenerating neurons (31). After CCI, the number of FJC-positive cells was decreased at 24 hours in the CCI + KD group versus the CCI + SC group (Figure 7, A and B). For evaluation of the functional outcome, we used balance beam and Morris water maze (MWM) tests. Balancing ability did not differ between groups before surgery (Figure 7C), suggesting that pretraining was consistent among both groups. However, after injury, a significantly better motor performance was observed on days 4 to 5 in the CCI + KD group compared with the CCI + SC group (Figure 7C). The results of the MWM tests also revealed that the CCI + KD rats performed better than the CCI + SC group on days 14–15 (Figure 7D).

Discussion

CLs are unusual tetra-acylated, triglycerol-bridged, and doubly negatively charged phospholipids presenting exclusively in the IMM (32–34). In eukaryotic cells, CLs are present exclusively in mitochondria, where they are essential for the structural, bioenergetics, and signaling functions (10, 35). Not surprisingly, disturbed CL metabolism leads to mitochondrial dyshomeostasis (33, 36). Apart from this, collapse of CL asymmetry and its appearance on the surface of mitochondria due to membrane depolarization act a

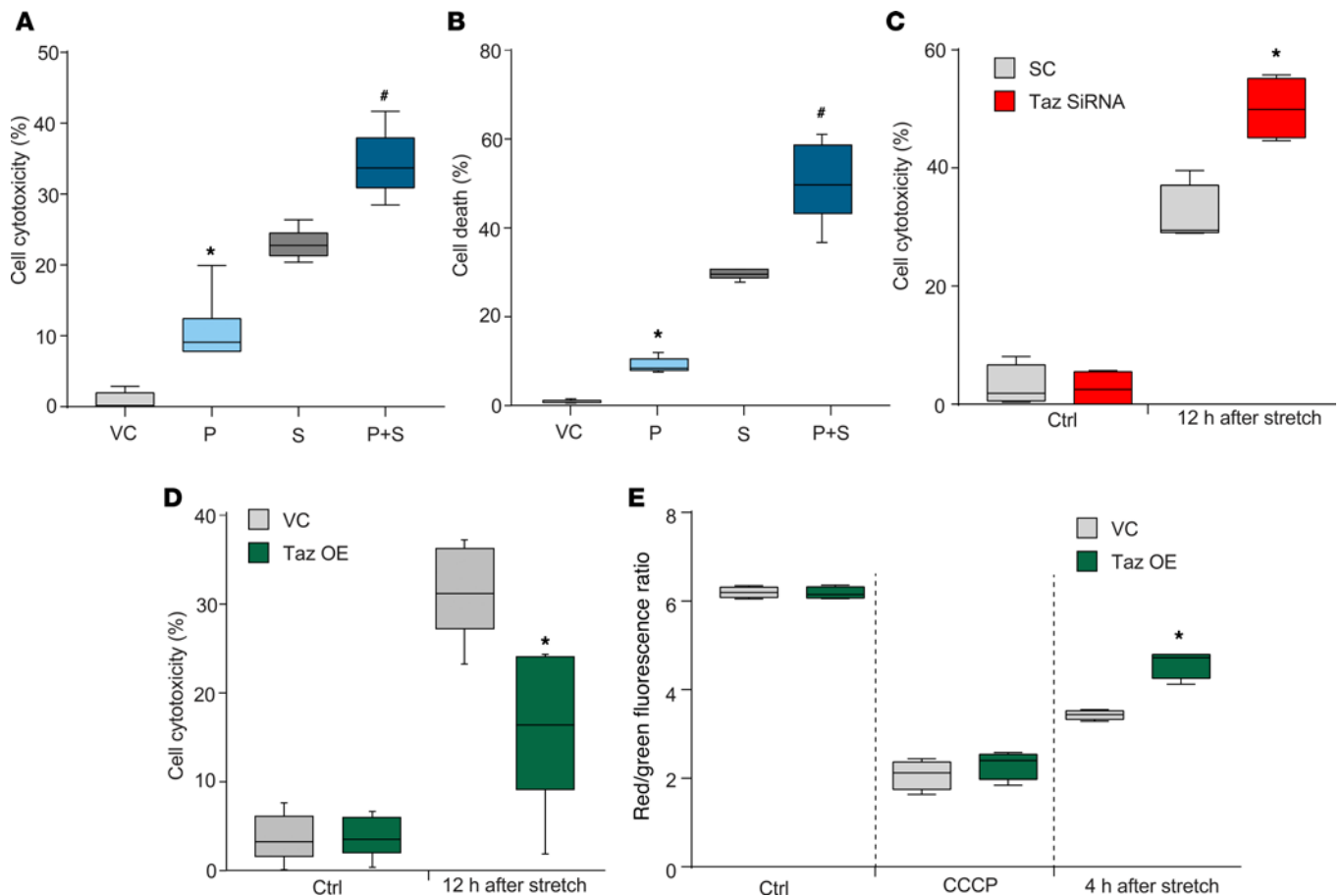


Figure 5. Neuronal cell death is influenced by the CL-remodeling pathway after mechanical stretch injury. (A) Quantification of cytotoxicity by CCK8 at 48 hours after transient transfection with iPLA₂ γ plasmid (P) and at 24 hours after stretch (S). Transfection efficiency was measured by Western blot analysis at 48 hours. $n = 6/\text{group}$, $*P < 0.05$ vs. vector control (VC), $*P < 0.05$ vs. vector plus S (vector + S), 1-way ANOVA. (B) Cell death measured by Annexin V-APC/7-AAD at 48 hours after transient transfection with P and at 24 hours after stretch. $n = 3/\text{group}$, $*P < 0.05$ vs. VC; $*P < 0.05$ vs. S by 1-way ANOVA. P, iPLA₂ γ overexpression group. S, Stretch group; P+S, iPLA₂(gamma) overexpression + stretch group (C) Quantification of cytotoxicity in Taz siRNA KD cells after stretch injury. $n = 4/\text{group}$, $*P < 0.05$ vs. scrambled siRNA control (SC), 1-way ANOVA. (D) Effect of Taz overexpression (OE) on mechanical stretch-induced cytotoxicity. $n = 3/\text{group}$, $*P < 0.05$ vs. VC, 1-way ANOVA. (E) Mitochondrial membrane potential measured by JC-1 in Taz-overexpressing and empty vector transfection cells after stretch injury. Carbonyl cyanide 3-chlorophenylhydrazone (CCCP) (10 μM) was used as a positive control. $n = 4/\text{group}$, $*P < 0.05$ vs. VC, 1-way ANOVA.

promitophagial signal leading to the elimination of injured mitochondria (37). Release of mitochondria with externalized CLs into extracellular environments and circulation represents triggers of immunogenic events affecting the pro- and antiinflammatory balance (38–40).

Metabolic modifications of CLs have been associated with mitochondrial dysfunction in several disease conditions, including a monogenic disease, Barth syndrome (41, 42). In Barth syndrome, the mutated gene of mCL reacylation — required for the normal remodeling and maturation of CL — is responsible for the development of cardiomyopathy and neutropenia, leading over time to mortality (43), and other less pronounced clinical manifestations, including a mild neurological impairment (44, 45). More robust effects have been linked with multiple metabolic misfortunes of CL, leading to its oxidation and hydrolysis (15, 46). On the cellular level, cytochrome *c*-catalyzed CL oxidation leads to massive apoptosis (47). Additionally, mCL accumulation has been shown to trigger mitochondrial binding of BH3-interacting domain death agonist, leading to apoptosis (48). A previous study showed that cervical cancer cells with disrupted mCL reacylation were more sensitive to apoptosis (49). The accumulated mCLs affect the physicochemical properties of the outer membrane and the proapoptotic action of Bcl-2 proteins, leading to membrane permeabilization (50). The increased mCL is also present in cerebral ischemia-reperfusion and Parkinson disease models, accompanied by CL oxidation (30, 51). One can assume that a combination of CL redox modification with the hydrolysis of CLox products may cause synergistic deleterious effects (51).

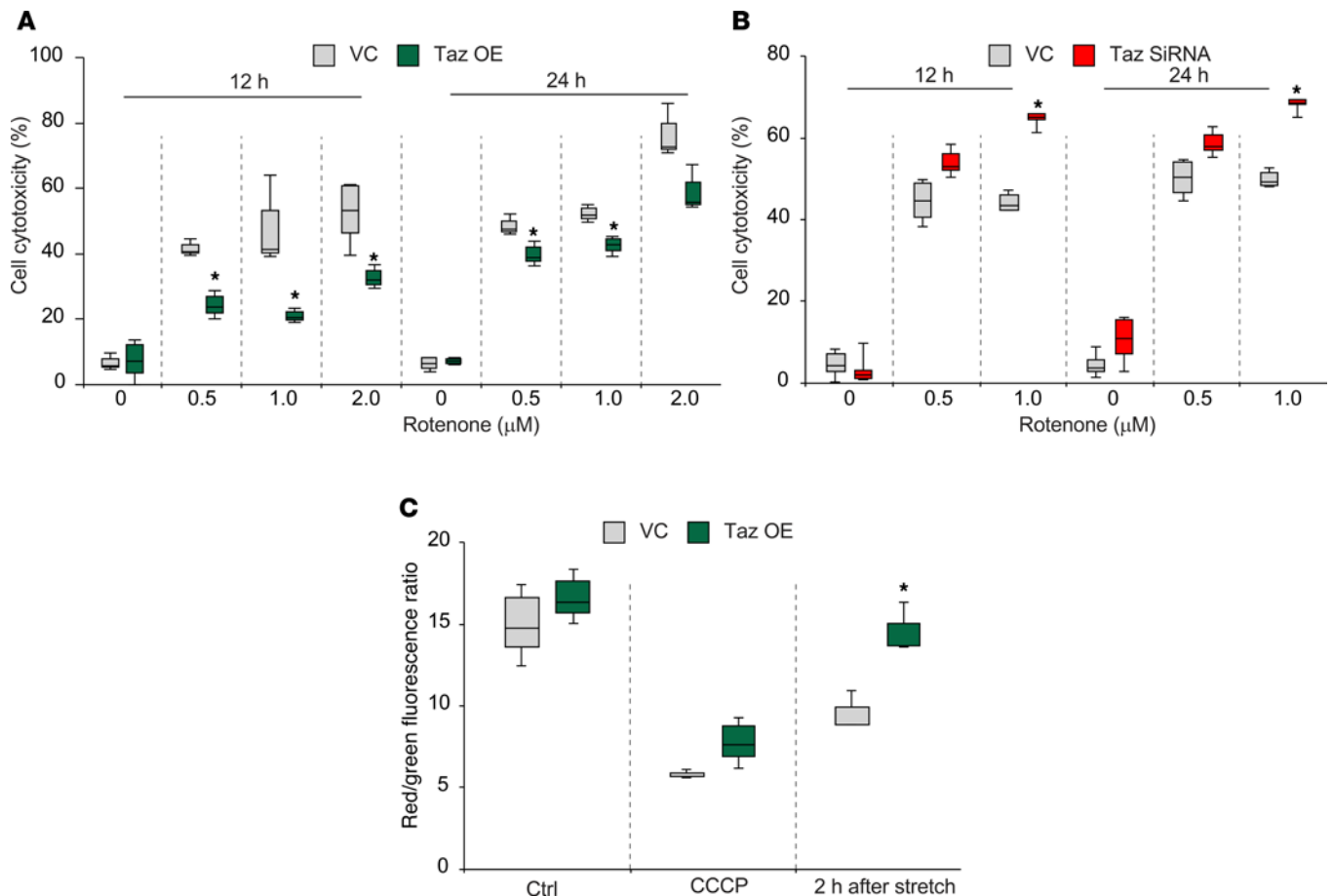


Figure 6. Taz deficiency enhances rotenone-induced neuronal injury. (A) Rotenone-induced cytotoxicity in Taz-transfected (Taz OE condition) or empty vector-transfected cells. $n = 3/\text{group}$, $*P < 0.05$ vs. VC group, 1-way ANOVA. The box plots depict the minimum and maximum values (whiskers), the upper and lower quartiles, and the median. The length of the box represents the interquartile range. (B) Rotenone-induced cytotoxicity in Taz siRNA or SC-transfected cells. $n = 5/\text{group}$, $*P < 0.05$ vs. SC group, 1-way ANOVA. (C) Mitochondrial membrane potential measured by JC-1 in Taz-overexpressing cells after rotenone ($1 \mu\text{M}$) treatment. CCCP ($10 \mu\text{M}$) was used as a positive control. $n = 3/\text{group}$, $*P < 0.05$ vs. VC group, 1-way ANOVA.

Brain trauma is a multifactorial injury with many mutually enhancing mechanisms of damage (52–54). Among those, mitochondrial damage with underlying CL metabolic disturbances has attracted attention as a potential target for new therapies (55). Notably, biochemically detectable prevention of CL oxidation has been demonstrated to be effective in the functional protection of the brain against traumatic injury (16). It is reasonable to expect that a combination therapy that also includes regulators of CL hydrolysis may yield nonlinear protective effects. However, the tightly intertwined redox and hydrolytic pathways of CL modification have not been untangled so far.

In the current work, using high-resolution LC-MS/MS, we showed for the first time to our knowledge that esterified PUFAs in CLs are targets of oxidation, which is followed by hydrolysis and formation of mCLs after TBI. A similar pattern of hydrolysis of PUFAs esterified into CLs and formation of mCLs was observed in Taz-deficient brains (Figure 4, C and D), where oxidation reactions that were seen in TBI did not complicate the picture. In response to mCL accumulation, there was an increase in the expression of the CL-remodeling enzyme Taz both in experimental and clinical TBI. Our data using an in vitro TBI model further supported the importance of CL hydrolysis and remodeling reactions in neuronal death by showing that overexpression of iPLA₂ γ and deficiency of Taz worsened neuronal survival. Combined with our previous observations (16, 52, 56), these data suggest an important, detrimental role for both CLox and mCL accumulation after TBI. It is likely that the combined presence of 2 types of “chaotropic” CL metabolites, CLox and mCL, synergistically enhances membrane damage after TBI. It is possible that a time-dosed therapeutic approach starting with regulators of CL oxidation, followed by regulators of hydrolysis, and then remodeling, will be particularly effective for improving outcomes after TBI.

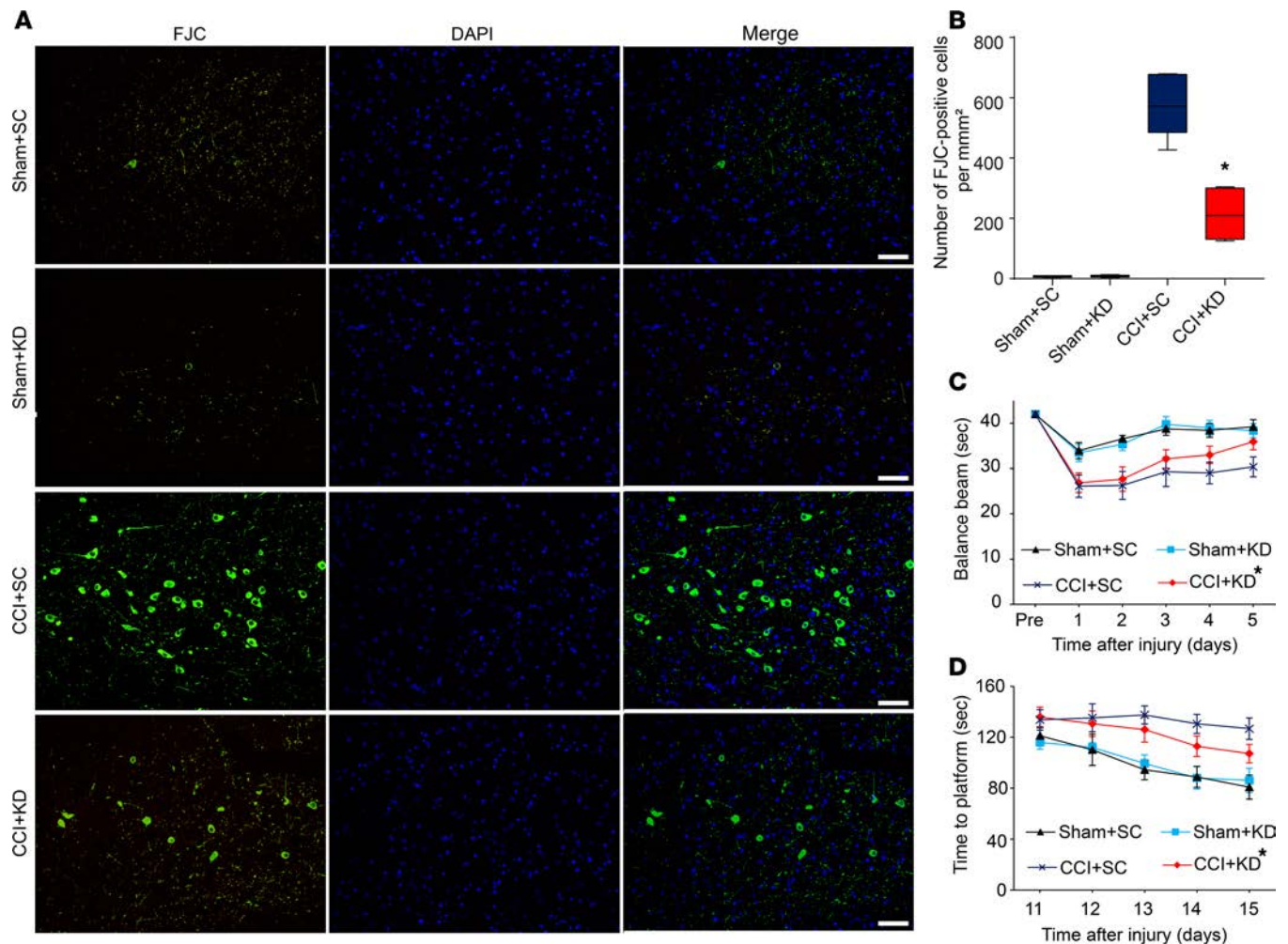


Figure 7. Deficiency of $iPLA_2\gamma$ attenuates TBI-induced neurodegeneration and behavioral deficits. (A) Representative images (of 6) showing neurodegeneration by Fluoro-Jade C (FJC) staining. (B) The number of FJC-positive cells observed in the injured cortex at 24 hours after CCI was attenuated by siRNA knock down of $iPLA_2\gamma$. The white scale bar represents 30 μm . $n = 6/\text{group}$, $*P < 0.05$ vs. CCI + SC, 1-way ANOVA. The box plots depict the minimum and maximum values (whiskers), the upper and lower quartiles, and the median. The length of the box represents the interquartile range. (C) Length of time (seconds) rats remain on the balance beam apparatus before and after CCI or sham injury, $n = 7/\text{group}$, $*P < 0.05$ vs. CCI + SC, 2-way ANOVA. (D) Latency (seconds) for rats to locate a hidden (submerged) platform on post-TBI days 11–15. $n = 7/\text{group}$, $*P < 0.05$ vs. CCI + SC, 2-way ANOVA.

The observed changes in the expression of CL hydrolysis and remodeling enzymes were similar, albeit greater, in the hippocampus than the contusional cortex (Supplemental Figure 5). The hippocampus is known to be selectively vulnerable to TBI, and trauma to it is partly responsible for the learning deficits observed after injury (57). Our lipidomics studies in the current work were focused on the contusional cortex. However, previous work using MALDI imaging revealed that decreases in PUFA-containing CLs is not limited to the contusional cortex in that the ipsilateral hippocampus suffers similar losses in highly unsaturated CL species (58), corroborating our findings regarding the expression of CL hydrolysis and remodeling enzymes in the current study.

Taz functions as a phospholipid and lysophospholipid acyltransferase (18). It is thought to play an important role in remodeling CLs in the heart, where the majority of CLs are homoacylated tetralinoleoyl CLs (17, 59, 60). In contrast, highly diversified heteroacylated CLs are typical of the brain (7). Mutations in the Taz gene lead to an accumulation of mCLs and a decrease in CLs in Barth syndrome patients (43). The major organs involved in Barth syndrome are the heart, the liver, and skeletal muscle, with minimal involvement of the CNS, resulting in mild learning disabilities and attention deficit as common features (41). The markedly greater learning deficits known to occur in the CCI model (61) suggest that CL oxidation is the major contributor to brain damage. This is further supported by improved neurobehavioral outcomes with the use of inhibitors of CL oxidation after acute CNS insults (16, 51).

Our results in Taz-deficient mice and mechanically injured rat brain are similar and show that PUFA-containing CLs are decreased and PUFA-containing mCLs are increased. Several studies demonstrated that Taz is not specific toward classes of donor phospholipids used for reacylation (62, 63). The abundant phospholipids, phosphatidylcholine and phosphatidylethanolamine, are the most common donors. Because Taz is known to have limited or no acyl chain selectivity (62, 63), these similarities suggest a common denominator: iPLA₂γ playing a major role in the generation of mCLs by hydrolysis of short-chain, relatively saturated fatty acids in the Taz-deficient brain and CLox in the injured brain. These data are in agreement with the known hydrolytic selectivity of the iPLA₂γ (20). Phospholipase A₂ enzymes have been widely studied in TBI, although this is the first study to our knowledge investigating the expression of mitochondrial iPLA₂γ after TBI. Previous studies in acute CNS injury showed significant increases in cytosolic PLA₂ after spinal cord injury (64). Our results indicating that overexpression of iPLA₂γ enhanced stretch-induced death of HT22 cells are in agreement with a deleterious role of iPLA₂γ in mitochondrial-mediated cell death (65). There has not been a study evaluating the neuroprotective potential of iPLA₂γ inhibitors after acute brain injury, although pretreatment with a selective inhibitor, (E)-6-(bromomethylene)-3-(1-naphthalenyl)-2H-tetrahydropyran-2-one (R-BEL), was shown to rescue myocardial ischemia-induced arrhythmia (66). Given the beneficial effects of Taz overexpression in improving survival of HT22 cells after mechanical stretch, it is possible that a combination strategy including iPLA₂γ inhibition and Taz upregulation could be more revealing.

In summary, we present, for the first time to our knowledge, evidence from quantitative assessment of peroxidation and hydrolysis of mitochondrial CLs that these 2 processes act as mutually enhancing components of the pathogenic mechanism of mitochondrial injury in TBI. This suggests that a time-dosed therapeutic approach starting with regulators of CL oxidation and followed by regulators of hydrolysis may be particularly effective in improving outcomes after TBI. Elimination of CLox via the hydrolysis and subsequent reacylation of mCLs formed may be maximally beneficial for the overall outcome. Thus, future efforts should be focused on the combined therapy with integrated enhancers of mCL reacylation. Because of the delayed hydrolysis compared with CL oxidation, there is an obvious therapeutic window for the development of new therapies for mCL reacylation.

Methods

Patients. Human brain tissue was obtained for analysis from the tissue bank of the Institutional Review Board–approved Department of Neurosurgery at the First Affiliated Hospital of Nanjing Medical University. Brain tissue resected from the pericontusional area of the temporal or frontal cortices of severe TBI patients who underwent decompressive craniectomy was flash frozen in liquid nitrogen and stored at –80°C until analysis. Brain tissue resected from the temporal cortices of epilepsy patients who underwent surgical treatment was used as a control and stored in the same manner as the TBI samples. Characteristics of the patients are described in Supplemental Table 1.

Animals. Postnatal day 10 Sprague-Dawley rat pups were obtained from Harlan Laboratories, Inc. and acclimated for a week before the experiments. Taz-KD mice were generated by mating male transgenic (Tg) mice [B6.Cg-Gt(ROSA)26Sortm1(1H)/tetO-RNAi:Taz,CAG-tetR)Bsf/ZkhuJ; The Jackson Laboratory], which have a doxycycline-inducible (dox-inducible) Taz-specific shRNA, with female C57BL/6J mice (The Jackson Laboratory) under a protocol approved by the University of Manitoba Animal Policy and Welfare Committee. All animals were maintained in an environmentally controlled facility (12-hour light/12-hour dark cycle), with free access to food and water. Experimental animals' Taz knock down was induced in utero and maintained postnatally by administering dox (625 mg/kg chow) as part of the standard low-fat (6% fat [w/w]) rodent chow (rodent diet catalog TD.01306; Harlan [now Envigo]; ref. 67). Female C57BL/6J mice consumed the dox diet (TD.01306) for at least 4 days before breeding. A low-fat diet lacking dox was used during the 4-day mating period to prevent Taz knock down in the Tg males. Dams were then returned to the dox diet (TD.01306) for their entire pregnancy, birth, and suckling period. Only male offspring were used experimentally; they were weaned at 3 weeks of age onto the low-fat (6% w/w) (rodent diet catalog TD.01306; Harlan) containing dox (625 mg/kg chow). Male mice positive for the Taz shRNA transgene were identified by PCR using primers (forward: 59-CCATGGAATTCGAA CGCTGACGTC-39; reverse: 59-TATGGGCTATGAACTAAT GACCC-39) as previously described (67). Nontransgenic littermates treated with a dox diet were used as WT controls. Brains were harvested at 4 months of age.

CCI model. The CCI model was performed as described previously (52). Briefly, a craniotomy was made over the left parietal cortex in the 17-day-old male Sprague-Dawley rats. Rats were anesthetized with

3.5% isoflurane in O₂ and maintained on 2% isoflurane in N₂O/O₂ (2:1). For all studies, a 6-mm, metal, pneumatically driven impactor tip was used; velocity was 4.0 ± 0.2 m/s, depth of penetration was 2.5 mm, and duration of deformation was 50 ms. After TBI, the bone flap was replaced and sealed with dental cement, and the scalp incision was closed. The rats were weaned from mechanical ventilation, extubated, and returned to their cages until sacrifice at 1, 4, or 24 hours after injury.

Cell culture of in vitro TBI and rotenone injury model. HT22 cells were a gift from David Schubert (The Salk Institute, La Jolla, California, USA). HT22 cells were seeded at 2 × 10⁴ cells/cm² and maintained in a monolayer culture in RPMI-1640 medium supplemented with 10% FBS for 24 hours before treatments and injury, with media changes every 2 days. Sterile technique was strictly followed in all procedures. In vitro TBI was produced using an established model of mechanical stretch (56). Briefly, HT22 cells cultured on silicone membranes were subjected to a computer-controlled, quantifiable, mechanical insult by displacing the membrane over a hollowed platform. The membranes were stretched with a known pre-tension across the surface of custom-designed, stainless steel wells that fit into the cell stretch apparatus. Cultures were subjected to a severe mechanical stretch, consisting of a rapid-onset strain pulse (10 pulse per second strain rate and 50% membrane deformation). In experiments involving rotenone, the compound was dissolved in DMSO at 0.5 μM, 1 μM, and 2 μM concentrations and incubated with HT22 cells in 10% FBS DMEM medium. As a positive control, cells were treated with CCCP (10 μM).

Lipid extraction, mass spectrometry (MS), and MS data analysis. The contusional cortex was isolated from the brain, and the lipids were extracted using Folch method. The total phosphate content of the lipids was quantified as described previously (68). For phospholipid analysis, samples corresponding to approximately 2.5 nmol of total phosphate were added with the appropriate internal standards (5 pmol each of phosphatidylcholine [17:0/17:0], phosphatidylglycerol [17:0/17:0], phosphatidylinositol [16:0/16:0], cardiolipin [14:0/14:0/14:0/14:0], phosphatidylserine [17:0/17:0], phosphatidic acid [17:0/17:0], and phosphatidylethanolamine [17:0/17:0]) and analyzed using LC-MS/MS. LC-MS analysis was performed using a Dionex Ultimate 3000 RSLCnano system coupled online to a Q-Exactive plus hybrid Quadrupole-Orbitrap mass spectrometer (Thermo Fisher Scientific) using a normal phase column (Luna 3 μm Silica [2], 100 Å, 150 × 2 mm [Phenomenex]). A multistep gradient with solvents A (hexane propanol/water/triethylamine/formic acid, 43:57:1:0.5:0.01 v/v containing 10 mM ammonium acetate) and B (hexane propanol/water/triethylamine/formic acid, 43:57:1:0.5:0.01 v/v containing 10 mM ammonium acetate) was used as follows: 0- to 15-min linear gradient from 10% B to 37% A at 200 μl/min, 15- to 23-min linear gradient from 37% to 40% B at 200 μl/min, 23- to 25-min linear gradient from 40% to 100% B at a linear increase in flow rate from 200 to 225 μl/min, 27- to 47-min isocratic at 100% B at 225 μl/min, 47- to 57-min linear gradient from 100% to 10% B with a linear decrease in flow rate from 225 to 200 μl/min, followed by re-equilibration of the column for 13 min with 10% solvent B at 200 μl/min. The mass spectra were acquired through data-dependent acquisition with a negative ion mode from 0 to 57 min. The spray voltage was set as 3.2 kv with a sheath gas flow rate of 10 AU. The spectra were recorded at 70,000 full width at half maximum resolution between 360 and 1,600 *m/z*, with the top 10 ions selected for fragmentation. Higher energy collisional dissociation fragmentation with 24 normalized collision energy was used while the ions were isolated at a ± 1 *m/z* isolation window.

FFAs were analyzed using reverse phase LC-MS/MS. Briefly, a sample equivalent to 2.5 nmol of the total phosphate was added with 100 pmol of internal standard C (17:0) and dissolved in 20 μl of methanol. Samples (0.5 μl) were injected into a reverse phase C18 column (Acclaim PepMap 100 C18, 2 μm, 100 Å, 150 × 0.3 mm) and eluted using a multistep gradient of solvent A (20% methanol in water containing 5 mM ammonium acetate) and solvent B (90% methanol in water containing 5 mM ammonium acetate). The following gradient steps with 12 μl/min flow rate were used: 0- to 70-min linear gradient from 30% to 95% solvent B; 70- to 90-min isocratic flow at 95% B; 80- to 83-min linear gradient from 30% to 95% B; and 83- to 90-min re-equilibration of the column at 30% B. The mass spectra data were analyzed using SIEVE 2.1 software (Thermo Fisher Scientific) using a database developed in house. Briefly, the exact masses of CL species containing various fatty acyl combinations were calculated theoretically. All isobaric and isomeric species were grouped into sum composition (total acyl chain carbon/double bond) in the CL database. The CLox database was developed from CL database by performing theoretical oxidation of all oxidizable (PUFA-containing) CL species. All ions within 7 ppm of calculated masses that were eluted within 5 min of CL internal standard (IS) species were identified using SIEVE 2.1 software. The identified lipids were confirmed by analyzing fragmentation of representative ions within the retention time range. The amounts of individual species were calculated using a calibration curve created with IS and varying concentrations of tetralinoleoyl-CL.

In vitro genetic modulation of the CL-remodeling pathway. Human *PNPLA8* cDNA (gene name of $iPLA_2\gamma$) was synthesized in the pEGFP-C1 vector by GENEWIZ, Inc. Cells were transfected with 60 nmol of plasmid using Lipofectamine 2000 (Invitrogen). The efficacy of *PNPLA8* was assessed by Western blot analysis using antibodies to $iPLA_2\gamma$ and GFP imaging. The plasmid double enzyme digestion and imaging were performed to verify plasmid and transfection efficiency. Experiments were performed 48 hours after transfection.

To overexpress Taz, we used Taz Lentiviral Activation Particles from Santa Cruz Biotechnology, Inc. (catalog number: sc-426211-LAC). Briefly, 10,000 HT22 cells/well were cultured on a 6-well plate. The medium was removed on day 2 and replaced with Polybrene (Sigma-Aldrich), followed by the addition of Lentiviral Activation Particles. The medium was changed with standard medium on day 3. Puromycin dihydrochloride, hygromycin B, and Blasticidin S HCl were added to the medium on day 5 to select Taz-overexpressing cells. Western blot was used to measure the transfection efficiency.

We used siRNA (Thermo Fisher Scientific siRNA IDs 184026, 86914, and 184028) to knock down Taz expression in HT22 cells. Cells were transfected with 60 nmol of plasmid using Lipofectamine 3000 (Invitrogen). The efficacy of Taz knock down was assessed by Western blot using antibodies to Taz (Santa Cruz Biotechnology, Inc., sc-365810). Experiments were performed 48 hours after transfection.

Assessment of cell cytotoxicity. Cells in the logarithmic phase of growth were seeded at 10,000 per well in 96-well plates, 6-well plates, or special stretch apparatus plates. Cell proliferation was assayed at the indicated time points using a CCK8 kit (Dojindo Laboratories, Co., Ltd.) according to the manufacturer's instructions.

Assessment of cell death. Flow cytometry (FC500; Beckman Coulter) detection of Annexin V-APC/7-AAD (KGA1023-1026, KeyGEN) was used to assess cell death 20 hours after stretch injury. Annexin V-APC-positive and 7-AAD-positive cells were considered dead cells.

Assessment of mitochondrial membrane potential. Mitochondrial membrane potential was assessed using JC-1 (Abcam). Mitochondria with intact membrane potential concentrate JC-1 into aggregates that show red fluorescence. De-energized mitochondria cannot concentrate JC-1 and show green fluorescence. After stretch and rotenone treatment, cells were incubated with JC-1 (10 μ M) in media for 30 min in the dark and collected by scraping. After washing with PBS, cells were subjected to FACS analysis. The ratio of JC-1 aggregate (green) to monomer (red) intensity was calculated. As a positive control, cells were treated with CCCP (10 μ M).

Immunoblot analysis. Extracts for immunoblotting were obtained from brain tissues and cells homogenized in RIPA buffer. In brief, proteins were separated by electrophoresis and then transferred to PVDF membranes by electroblotting. The primary antibodies were $iPLA_2\gamma$ (1:200; Santa Cruz Biotechnology, Inc., sc-241491), Taz (1:200; Santa Cruz Biotechnology, Inc., sc-100870 sc-365810), GAPDH (1:1,000; Cell Signaling Technology 5174), β -actin (1:2000; Abcam, ab6276), Tim23 (1:1000; Santa Cruz Biotechnology, Inc., sc-514463)

siRNA administration into the lateral ventricle. Sprague-Dawley rats for $iPLA_2\gamma$ -KD experiments were purchased from the animal core facility of Nanjing Medical University. The siRNA targeting the rat *PNPLA8* gene to knock down $iPLA_2\gamma$ expression in vivo was designed by Genewiz. Osmotic minipumps were filled with 30 nmol siRNA for infusion at a rate of 1.0 μ l/day for 72 hours. A brain infusion cannula was implanted into the left lateral ventricle (coordinates: -0.8 mm posterior to bregma, -1.5 mm lateral to midline, and -4.6 mm ventral to the skull surface). The efficacy of the knock down of the targeted protein was evaluated by Western blot.

FJC staining. FJC (catalog number: AG325, Sigma-Aldrich) staining was performed as described (69). Briefly, the slides were stained with 0.001% FJB solution and dried in oven in the dark for over 1 hour before being cleared by immersion in xylene and coverslipped. The dried slices were immersed in xylene for at least 1 min and then were covered by neutral gum. The slides were observed and photographed under a fluorescence microscope. The nuclei were stained with DAPI and showed blue fluorescence. FJC-positive cells (green signal) were counted from 5 randomly chosen fields, and the average number of cells was calculated.

Assessments of motor function and cognitive performance. Motor function was evaluated using balance beam testing, which was performed on postinjury days 1–5 by the same experienced investigator blinded to the experimental group assignment, as described previously (70). Rats were grasped by the tail and placed on a wooden beam suspended between 2 upright bars. The amount of time for which rats could remain (in seconds) on the balance beam was recorded and analyzed using Prism Software 6.04 (GraphPad Software, Inc.).

For the MWM, the water temperature was maintained at $25 \pm 2^\circ\text{C}$. To ensure recovery from motor deficits, hidden platform testing was performed on post-TBI days 11–15. Rats were allowed a maximum of 120 seconds to look for the submerged platform. If rats failed to reach the platform within 120 seconds, the experimenter placed them on the platform for 15 seconds. There was a minimum of 5 min between each

trial and each rat was given two trials per day. The latencies for rats to reach the platform were recorded using a tracking device (ANY-maze software), and the data were analyzed by 2-way ANOVA using Prism Software 6.04 (GraphPad Software, Inc.).

Statistics. All experimental data except the functional outcome results are expressed as mean \pm SD and were analyzed by 2-tailed Student's *t* test (for comparison of 2 groups) or 1-way ANOVA (for comparison of > 2 groups), followed by Fisher's post hoc analysis using Prism Software 6.04 (GraphPad Software, Inc.). Differences were considered statistically significant when the *P* value was less than 0.05. The motor and MWM data are presented as the mean \pm SEM and were analyzed by 2-way ANOVA using Prism Software 6.04 (GraphPad Software, Inc.) for overall significance, followed by Bonferroni-Dunn post hoc test for between-group comparisons. A *P* value of less than 0.05 was considered significant.

Study approval. Human brain samples were obtained from the collection of the Department of Neurosurgery at the First Affiliated Hospital of Nanjing Medical University. All procedures were preapproved and performed according to the protocols established by the Medical Ethics Review Board of Nanjing Medical University. Informed consent was obtained from the patients or their legal representatives before participation began. Procedures concerning transgenic mice conformed to the Canadian Council on Animal Care, and use of the mice was approved by the University of Manitoba Animal Protocol Committee. All experimental procedures performed in PND17 rats were preapproved and performed according to the protocols established by the Institutional Animal Care and Use Committee at the University of Pittsburgh. All iPLA2 γ -KD *in vivo* experiments were approved by Nanjing Medical University Animal Care and Use Committee.

Author contributions

HC and TSA designed the experiments, analyzed the data, and wrote the manuscript. HC, TSA, EMK, and AAA performed *in vivo* and *in vitro* experiments including the TBI model, genetic cell line construction, cell stretch injury, Western blot analysis, and cell toxicity test. TSA, EMK, and AAA contributed to the lipid extraction and LC-MS data analysis. LKC and GMH contributed to the Taz-KD mouse experiments. HB, VEK, and JJ initiated and directed the entire study, designed experiments, and wrote the manuscript.

Acknowledgments

We thank Henry Alexander and Jessie Lewis for technical support in the CCI experiments. This work was supported by the NIH (HL114453, AI068021, NS076511, NS061817, NS084604, and CA165065), Human Frontier Science Program (HFSP-RGP0013/2014), Heart and Stroke Foundation of Canada, Barth Syndrome Foundation Canada/USA, National Natural Science Foundation of China (81471269), Jiangsu Province's Natural Science Foundation (BK20160047), and Jiangsu Province and the Priority Academic Program Development of Jiangsu Higher Education Institutions (PAPD). GMH is the Canada Research Chair in Molecular Cardiolipin Metabolism.

Address correspondence to: Jing Ji, Department of Neurosurgery, The First Affiliated Hospital of Nanjing Medical University, 300 Guangzhou Rd, Nanjing 210029, Jiangsu Province, China. Phone: 86.13912976265; Email: jijing@njmu.edu.cn. Or to: Valerian E. Kagan, Department of Environmental and Occupational Health, Public Health Building, 130 De Soto St, Pittsburgh, Pennsylvania 15261, USA. Phone: 412.624.9700; Email: kagan@pitt.edu. Or to: Hülya Bayır, Department of Critical Care Medicine, University of Pittsburgh, John G. Rangos Research Center- 6th Floor, 4401 Penn Avenue, Pittsburgh, Pennsylvania 15224, USA. Phone: 412.383.7865; E-mail: bayihx@ccm.upmc.edu.

1. Bruns J Jr, Hauser WA. The epidemiology of traumatic brain injury: a review. *Epilepsia*. 2003;44(s10):2–10.
2. Feigin VL, et al. Incidence of traumatic brain injury in New Zealand: a population-based study. *Lancet Neurol*. 2013;12(1):53–64.
3. Lifshitz J, Sullivan PG, Hovda DA, Wieloch T, McIntosh TK. Mitochondrial damage and dysfunction in traumatic brain injury. *Mitochondrion*. 2004;4(5–6):705–713.
4. Singh IN, Sullivan PG, Deng Y, Mbye LH, Hall ED. Time course of post-traumatic mitochondrial oxidative damage and dysfunction in a mouse model of focal traumatic brain injury: implications for neuroprotective therapy. *J Cereb Blood Flow Metab*. 2006;26(11):1407–1418.
5. Schlame M, Ren M. The role of cardiolipin in the structural organization of mitochondrial membranes. *Biochim Biophys Acta*. 2009;1788(10):2080–2083.
6. Paradies G, Paradies V, De Benedictis V, Ruggiero FM, Petrosillo G. Functional role of cardiolipin in mitochondrial bioenergetics. *Biochim Biophys Acta*. 2014;1837(4):408–417.

7. Kagan VE, et al. Cardiolipin signaling mechanisms: collapse of asymmetry and oxidation. *Antioxid Redox Signal*. 2015;22(18):1667–1680.
8. Kagan VE, et al. Cytochrome c/cardioliipin relations in mitochondria: a kiss of death. *Free Radic Biol Med*. 2009;46(11):1439–1453.
9. Kagan VE, Chu CT, Tyurina YY, Cheikhi A, Bayir H. Cardiolipin asymmetry, oxidation and signaling. *Chem Phys Lipids*. 2014;179:64–69.
10. Claypool SM, Koehler CM. The complexity of cardiolipin in health and disease. *Trends Biochem Sci*. 2012;37(1):32–41.
11. Kagan VE, et al. Oxidative lipidomics of apoptosis: redox catalytic interactions of cytochrome c with cardiolipin and phosphatidylserine. *Free Radic Biol Med*. 2004;37(12):1963–1985.
12. Sedláč E, Robinson NC. Phospholipase A(2) digestion of cardiolipin bound to bovine cytochrome c oxidase alters both activity and quaternary structure. *Biochemistry*. 1999;38(45):14966–14972.
13. Buland JR, et al. Biosynthesis of oxidized lipid mediators via lipoprotein-associated phospholipase A2 hydrolysis of extracellular cardiolipin induces endothelial toxicity. *Am J Physiol Lung Cell Mol Physiol*. 2016;311(2):L303–L316.
14. Tyurina YY, et al. Characterization of cardiolipins and their oxidation products by LC-MS analysis. *Chem Phys Lipids*. 2014;179:3–10.
15. Tyurina YY, et al. A mitochondrial pathway for biosynthesis of lipid mediators. *Nat Chem*. 2014;6(6):542–552.
16. Ji J, et al. Lipidomics identifies cardiolipin oxidation as a mitochondrial target for redox therapy of brain injury. *Nat Neurosci*. 2012;15(10):1407–1413.
17. Houtkooper RH, et al. The enigmatic role of tafazzin in cardiolipin metabolism. *Biochim Biophys Acta*. 2009;1788(10):2003–2014.
18. Xu Y, Malhotra A, Ren M, Schlame M. The enzymatic function of tafazzin. *J Biol Chem*. 2006;281(51):39217–39224.
19. Xu Y, Kelley RI, Blanck TJ, Schlame M. Remodeling of cardiolipin by phospholipid transacylation. *J Biol Chem*. 2003;278(51):51380–51385.
20. Tyurina YY, et al. Lipidomics characterization of biosynthetic and remodeling pathways of cardiolipins in genetically and nutritionally manipulated yeast cells. *ACS Chem Biol*. 2017;12(1):265–281.
21. Taylor WA, Hatch GM. Identification of the human mitochondrial linoleoyl-coenzyme A monolysocardiolipin acyltransferase (MLCL AT-1). *J Biol Chem*. 2009;284(44):30360–30371.
22. Taylor WA, Mejia EM, Mitchell RW, Choy PC, Sparagna GC, Hatch GM. Human trifunctional protein alpha links cardiolipin remodeling to beta-oxidation. *PLoS One*. 2012;7(11):e48628.
23. Murakami M, et al. Group VIB Ca²⁺-independent phospholipase A2 γ promotes cellular membrane hydrolysis and prostaglandin production in a manner distinct from other intracellular phospholipases A2. *J Biol Chem*. 2005;280(14):14028–14041.
24. Moon SH, Jenkins CM, Liu X, Guan S, Mancuso DJ, Gross RW. Activation of mitochondrial calcium-independent phospholipase A2 γ (iPLA2 γ) by divalent cations mediating arachidonate release and production of downstream eicosanoids. *J Biol Chem*. 2012;287(18):14880–14895.
25. Li N, et al. Mitochondrial complex I inhibitor rotenone induces apoptosis through enhancing mitochondrial reactive oxygen species production. *J Biol Chem*. 2003;278(10):8516–8525.
26. Moon Y, Lee KH, Park JH, Geum D, Kim K. Mitochondrial membrane depolarization and the selective death of dopaminergic neurons by rotenone: protective effect of coenzyme Q10. *J Neurochem*. 2005;93(5):1199–1208.
27. Wang L, et al. Mitochondrial respiratory chain inhibitors involved in ROS production induced by acute high concentrations of iodide and the effects of SOD as a protective factor. *Oxid Med Cell Longev*. 2015;2015:217670.
28. Chen Q, Vazquez EJ, Moghaddas S, Hoppel CL, Lesnfsky EJ. Production of reactive oxygen species by mitochondria: central role of complex III. *J Biol Chem*. 2003;278(38):36027–36031.
29. Testa CM, Sherer TB, Greenamyre JT. Rotenone induces oxidative stress and dopaminergic neuron damage in organotypic substantia nigra cultures. *Brain Res Mol Brain Res*. 2005;134(1):109–118.
30. Tyurina YY, Winnica DE, Kapralova VI, Kapralov AA, Tyurin VA, Kagan VE. LC/MS characterization of rotenone induced cardiolipin oxidation in human lymphocytes: implications for mitochondrial dysfunction associated with Parkinson's disease. *Mol Nutr Food Res*. 2013;57(8):1410–1422.
31. Schmued LC, Albertson C, Slikker W. Fluoro-Jade: a novel fluorochrome for the sensitive and reliable histochemical localization of neuronal degeneration. *Brain Res*. 1997;751(1):37–46.
32. Chicco AJ, Sparagna GC. Role of cardiolipin alterations in mitochondrial dysfunction and disease. *Am J Physiol Cell Physiol*. 2007;292(1):C33–C44.
33. Lu YW, Claypool SM. Disorders of phospholipid metabolism: an emerging class of mitochondrial disease due to defects in nuclear genes. *Front Genet*. 2015;6:3.
34. Schlattner U, et al. Mitochondrial cardiolipin/phospholipid trafficking: the role of membrane contact site complexes and lipid transfer proteins. *Chem Phys Lipids*. 2014;179:32–41.
35. Kiebish MA, et al. Dysfunctional cardiac mitochondrial bioenergetic, lipidomic, and signaling in a murine model of Barth syndrome. *J Lipid Res*. 2013;54(5):1312–1325.
36. Ren M, Phoon CK, Schlame M. Metabolism and function of mitochondrial cardiolipin. *Prog Lipid Res*. 2014;55:1–16.
37. Chu CT, et al. Cardiolipin externalization to the outer mitochondrial membrane acts as an elimination signal for mitophagy in neuronal cells. *Nat Cell Biol*. 2013;15(10):1197–1205.
38. O'Neill LA. Cardiolipin and the Nlrp3 inflammasome. *Cell Metab*. 2013;18(5):610–612.
39. Chakraborty K, et al. The mito-DAMP cardiolipin blocks IL-10 production causing persistent inflammation during bacterial pneumonia. *Nat Commun*. 2017;8:13944.
40. Balasubramanian K, et al. Dichotomous roles for externalized cardiolipin in extracellular signaling: promotion of phagocytosis and attenuation of innate immunity. *Sci Signal*. 2015;8(395):ra95.
41. Saric A, Andreau K, Armand AS, Møller IM, Petit PX. Barth Syndrome: from mitochondrial dysfunctions associated with aberrant production of reactive oxygen species to pluripotent stem cell studies. *Front Genet*. 2015;6:359.
42. Aprikyan AA, Khuchua Z. Advances in the understanding of Barth syndrome. *Br J Haematol*. 2013;161(3):330–338.
43. Schlame M, Ren M. Barth syndrome, a human disorder of cardiolipin metabolism. *FEBS Lett*. 2006;580(23):5450–5455.
44. Adès LC, et al. Barth syndrome: clinical features and confirmation of gene localisation to distal Xq28. *Am J Med Genet*.

- 1993;45(3):327–334.
45. Christodoulou J, et al. Barth syndrome: clinical observations and genetic linkage studies. *Am J Med Genet.* 1994;50(3):255–264.
46. Schug ZT, Gottlieb E. Cardiolipin acts as a mitochondrial signalling platform to launch apoptosis. *Biochim Biophys Acta.* 2009;1788(10):2022–2031.
47. Kagan VE, et al. Cytochrome c acts as a cardiolipin oxygenase required for release of proapoptotic factors. *Nat Chem Biol.* 2005;1(4):223–232.
48. Esposti MD, Cristea IM, Gaskell SJ, Nakao Y, Dive C. Proapoptotic Bid binds to monolysocardiolipin, a new molecular connection between mitochondrial membranes and cell death. *Cell Death Differ.* 2003;10(12):1300–1309.
49. Chen M, Zhang Y, Zheng PS. Tafazzin (TAZ) promotes the tumorigenicity of cervical cancer cells and inhibits apoptosis. *PLoS One.* 2017;12(5):e0177171.
50. Crimi M, Esposti MD. Apoptosis-induced changes in mitochondrial lipids. *Biochim Biophys Acta.* 2011;1813(4):551–557.
51. Ji J, et al. Deciphering of mitochondrial cardiolipin oxidative signaling in cerebral ischemia-reperfusion. *J Cereb Blood Flow Metab.* 2015;35(2):319–328.
52. Bayir H, et al. Selective early cardiolipin peroxidation after traumatic brain injury: an oxidative lipidomics analysis. *Ann Neurol.* 2007;62(2):154–169.
53. Gennarelli TA. Mechanisms of brain injury. *J Emerg Med.* 1993;11(suppl 1):5–11.
54. Werner C, Engelhard K. Pathophysiology of traumatic brain injury. *Br J Anaesth.* 2007;99(1):4–9.
55. Kagan VE, et al. Mitochondrial targeting of electron scavenging antioxidants: Regulation of selective oxidation vs random chain reactions. *Adv Drug Deliv Rev.* 2009;61(14):1375–1385.
56. Ji J, et al. Mitochondrial injury after mechanical stretch of cortical neurons in vitro: biomarkers of apoptosis and selective peroxidation of anionic phospholipids. *J Neurotrauma.* 2012;29(5):776–788.
57. Girgis F, Pace J, Sweet J, Miller JP. Hippocampal neurophysiologic changes after mild traumatic brain injury and potential neuromodulation treatment approaches. *Front Syst Neurosci.* 2016;10:8.
58. Sparvero LJ, et al. Imaging mass spectrometry reveals loss of polyunsaturated cardiolipins in the cortical contusion, hippocampus, and thalamus after traumatic brain injury. *J Neurochem.* 2016;139(4):659–675.
59. Claypool SM, Whited K, Srijumnong S, Han X, Koehler CM. Barth syndrome mutations that cause tafazzin complex lability. *J Cell Biol.* 2011;192(3):447–462.
60. Ye C, Shen Z, Greenberg ML. Cardiolipin remodeling: a regulatory hub for modulating cardiolipin metabolism and function. *J Bioenerg Biomembr.* 2016;48(2):113–123.
61. Osier N, Dixon CE. The controlled cortical impact model of experimental brain trauma: overview, research applications, and protocol. *Methods Mol Biol.* 2016;1462:177–192.
62. Schlame M, et al. The physical state of lipid substrates provides transacylation specificity for tafazzin. *Nat Chem Biol.* 2012;8(10):862–869.
63. Schlame M, Xu Y, Ren M. The basis for Acyl specificity in the Tafazzin reaction. *J Biol Chem.* 2017;292(13):5499–5506.
64. Liu NK, et al. Cytosolic phospholipase A2 protein as a novel therapeutic target for spinal cord injury. *Ann Neurol.* 2014;75(5):644–658.
65. Moon SH, Jenkins CM, Kiebish MA, Sims HF, Mancuso DJ, Gross RW. Genetic ablation of calcium-independent phospholipase A(2) γ (iPLA(2) γ) attenuates calcium-induced opening of the mitochondrial permeability transition pore and resultant cytochrome c release. *J Biol Chem.* 2012;287(35):29837–29850.
66. Mancuso DJ, et al. Cardiac ischemia activates calcium-independent phospholipase A2 β , precipitating ventricular tachyarrhythmias in transgenic mice: rescue of the lethal electrophysiologic phenotype by mechanism-based inhibition. *J Biol Chem.* 2003;278(25):22231–22236.
67. Acehan D, et al. Cardiac and skeletal muscle defects in a mouse model of human Barth syndrome. *J Biol Chem.* 2011;286(2):899–908.
68. Tyurin VA, Yanamala N, Tyurina YY, Klein-Seetharaman J, Macphee CH, Kagan VE. Specificity of lipoprotein-associated phospholipase A(2) toward oxidized phosphatidylserines: liquid chromatography-electrospray ionization mass spectrometry characterization of products and computer modeling of interactions. *Biochemistry.* 2012;51(48):9736–9750.
69. Shellington DK, et al. Polynitroxylated pegylated hemoglobin: a novel neuroprotective hemoglobin for acute volume-limited fluid resuscitation after combined traumatic brain injury and hemorrhagic hypotension in mice. *Crit Care Med.* 2011;39(3):494–505.
70. Adelson PD, Dixon CE, Robichaud P, Kochanek PM. Motor and cognitive functional deficits following diffuse traumatic brain injury in the immature rat. *J Neurotrauma.* 1997;14(2):99–108.